Macromolecules

ARTICLE

pubs.acs.org/Macromolecules

Tailoring Crystallization Behavior of PEO-Based Liquid Crystalline Block Copolymers through Variation in Liquid Crystalline Content

Yuxiang Zhou,[†] Suk-kyun Ahn,[‡] Rubinder Kaur Lakhman,[‡] Manesh Gopinadhan,[§] Chinedum O. Osuji,[§] and Rajeswari M. Kasi*[,†,‡]

[†]Department of Chemistry, University of Connecticut, Storrs, Connecticut 06269, United States

[‡]Polymer Program, Institute of Materials Science, University of Connecticut, Storrs, Connecticut 06269, United States

[§]Department of Chemical and Environmental Engineering, Yale University, New Haven, Connecticut 06520, United States

Supporting Information

ABSTRACT: A series of liquid crystalline−semicrystalline−liquid crystalline triblock copolymers, with poly(ethylene oxide) (PEO) as the semicrystalline central block and polymethacrylate bearing side-chain cholesteryl mesogens as the liquid crystalline (LC) end blocks, are prepared using reversible addition−fragmentation chain transfer (RAFT) polymerization. Starting with 20 kg/mol PEO, the weight fractions of the LC blocks in the triblock copolymers are varied from 21 to 86 wt %. The wide-angle and small-angle X-ray scattering (WAXS and SAXS) as well as transmission electron microscopy (TEM) studies show that with the increased LC content in the triblock copolymers different hierarchical structures including "LC lamellae in PEO lamellae" and "PEO cylinders in LC matrix" are observed sequentially. Differential scanning calorimetry (DSC) study shows that the triblock copolymers with "LC lamellae in PEO lamellae" crystallize at normal undercooling conditions (crystallization temperature T_c observed at 31.0−36.4 °C, which is close to that of homopolymer PEO), while those with "PEO cylinders in LC matrix" crystallize at very large undercooling (T_c drops to −23.5 to −27.8 °C). The large variation of the undercooling conditions required for PEO crystallization is attributed to the nanoconfinement effect from different hierarchical structures at varied LC contents. Avrami analysis has been performed to understand the PEO crystallization mechanism. In "LC lamellae in PEO lamellae", the PEO crystallization is confined within 2D microdomains between LC lamellae and follows heterogeneous nucleation mechanism with subsequent long-range crystal growth. In "PEO cylinders in LC matrix", the PEO crystallization is confined within 1D cylindrical microdomains and dominated by homogeneous nucleation, and long-range crystal growth is prohibited by the surrounding LC matrix. This study demonstrates that microsegregated LC domains can provide efficient confinement of the PEO crystallization, and by simply increasing the LC content, amorphous PEO can be obtained at room temperature. These LC−semicrystalline−LC triblock copolymers, with room temperature amorphous PEO confined in microsegregated nanodomains, may be used as scaffolds for lithium ion batteries and solid-state electrolytes.

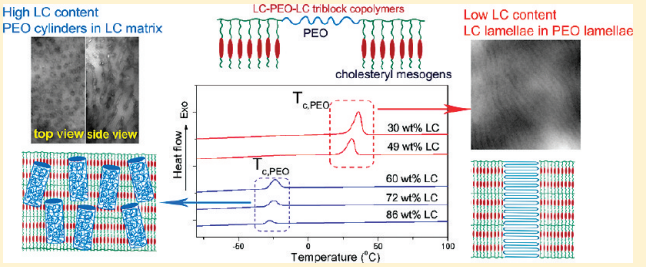

INTRODUCTION

Poly(ethylene oxide) (PEO) is a good candidate for solid-state electrolyte in lithium batteries. The ether oxygen in PEO can coordinate with doped lithium ions, and the segmental motion continuously creates new coordination sites to induce ion transport.[1−3] However, as a semicrystalline polymer, the crystals of PEO will reduce the segment and chain mobility, and this, in turn, decreases the ionic conductivity of the polyelectrolyte.[4] Block copolymers (BCP) containing PEO helps to overcome this problem by allowing the use of molten amorphous PEO for ion transport at elevated temperature while the block copolymer architecture helps retain the mechanical integrity of the whole material.[5−9] Furthermore, the self-assembled microsegregated structures of BCPs may provide nanosized pathways for ion transport.[6,9−13] Nevertheless, to meet the practical needs of using the polymer electrolyte at ambient temperature, producing PEO of lowered crystallinity at room temperature is crucial. Crystallinity of PEO can be reduced by doping lithium salts into PEO. However, increasing the content of the lithium ions beyond a critical concentration results in the formation of PEO/lithium ion crystalline complex, which increases the glass transition temperature (T_g) of the material.[1−3,10,11] It is also shown that doping poly(acrylic acid) (PAA) into PEO-based block copolymers can suppress the PEO crystallization and strengthen the microphase separation, due to the formation of interpolymer complexes between PAA and PEO through hydrogen bonding.[12,14] However, relatively high PAA content (25−40 wt % with respect to PEO) is required to achieve this purpose.[12,14] Whether this

Received: December 22, 2010
Revised: March 30, 2011
Published: April 25, 2011

high content of PAA will occupy too many lone pairs of ether oxygen and subsequently hinder the coordination bonding between lithium ions and PEO is yet to be reported.

It is well-known that PEO crystallization behavior can be tailored by confining PEO in restricted domains such as microdroplets,[15−18] thin films,[19−27] or block copolymer microsegregated structures.[28−32] Specifically, PEO crystallization can be confined within the block copolymer microsegregated domains when the noncrystalline block is stiff (glassy material) or the microsegregation between PEO and the noncrystalline block is very strong (large χ parameter), so that PEO crystals cannot disrupt or penetrate through the preformed microsegregated domains during crystallization.[33−35] The confined PEO crystallization mechanism strongly depends on the geometry and continuity of the microsegregated morphology as well as the T_g of the noncrystalline block.[32,34] Extensive studies on the confined PEO crystallization behaviors of PEO-amorphous BCPs have been reported. While confined PEO domain often shows a suppressed crystallization mechanism, only a few have achieved amorphous PEO at room temperature.[34−36] For instance, Zhu et al. have done intensive investigation on the PEO crystallization behaviors of polystyrene-*b*-PEO.[30−33,37,38] They have found that isolated nanostructures such as cylinders and gyroids provide stronger confinement to PEO crystallization compared to continuous lamellar structure, resulting in lower crystallization temperature and crystallinity.[37] Nevertheless, amorphous PEO domain at room temperature is not obtained in this system. In another example, Chen et al. have obtained amorphous PEO domain in PEO-*b*-poly(1,4-butadiene)/poly(1,4-butadiene) blends with high poly(1,4-butadiene) volume fractions (f = 0.69−0.87). At these high volume fractions, the isolated cylindrical or spherical structures are formed which prevent long-range crystal growth for PEO, leading to exceedingly large undercooling of crystallization (crystallization temperature T_c much lower than room temperature).[34]

Unlike semicrystalline−amorphous BCPs, the nanoconfinement of semicrystalline blocks in liquid crystalline (LC)−semicrystalline BCPs have not been thoroughly investigated. Sidechain liquid crystalline block copolymers (SCLCBCPs) are known to form hierarchical structures, that is, BCP microphase separation (e.g., spheres, cylinders, or lamellae) at around 10−100 nm length scale with LC ordering confined in microsegregated domains.[39−47] It can be envisioned that in PEO containing SCLCBCPs the presence of LC structure may strengthen the confinement effect of PEO crystallization because the formation of long-range PEO crystals will need to disrupt the preformed ordered LC domain. To date, many PEO based LC-semicrystalline BCPs have been prepared.[48−54] However, detailed phase investigation based on (i) the presence of hierarchical structure on the overall morphology, (ii) the interplay of LC ordering and PEO crystallization, and (iii) the resulting confined PEO crystallization mechanism is yet to be studied. The LC phase is responsive to external electric and magnetic fields, which makes the alignment of the amorphous PEO domain possible.[12,42,52,55,56] A recent publication by Osuji et al. demonstrates a method of aligning a LC-PEO BCP containing cyanobiphenyl mesogens with magnetic field. The resulting highly anisotropic cylindrical PEO domains doped with lithium salts show significantly increased conductivity.[13]

We have prepared a series of LC−semicrystalline−LC triblock copolymers with a PEO block of 20 kg/mol molecular weight as the central block and polymethacrylate bearing cholesteryl mesogens as the LC end blocks. By varying the weight fraction of the LC block, different hierarchical structures are obtained, providing different extents of nanoconfinement to PEO block. Increasing the LC content leads to exceedingly large undercooling for PEO crystallization and thus amorphous PEO can be obtained at room temperature without adding any other dopants or additives. This study provides a practical method of exploiting hierarchical structures to tailor PEO crystallization behavior.

Scheme 1. Synthesis of Monomer and Triblock Copolymers

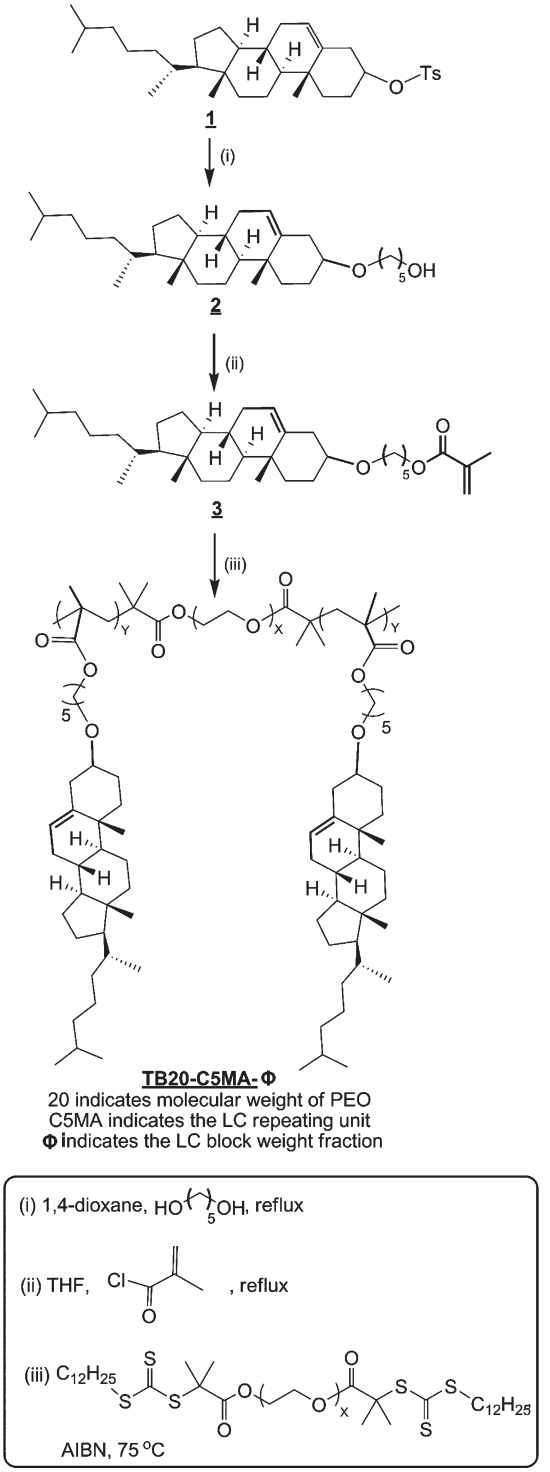

Table 1. Preparation of Macromolecular Chain Transfer Agent and Triblock Copolymers

polymer	CTA−PEO−CTA:C5MA[a]	$M_{n,GPC}$ (g/mol)[b]	PDI[b]	wt % of LC block[c]
CTA-PEO-CTA	NA	15 059	1.06	NA
TB20-C5MA-21	2:1	18 057	1.08	21
TB20-C5MA-30	1:1	22 957	1.11	30
TB20-C5MA-49	1:2	28 812	1.17	49
TB20-C5MA-60	1:3	37 983	1.26	60
TB20-C5MA-72	1:4	42 315	1.35	72
TB20-C5MA-86	1:6	56 060	1.40	86

[a] Feed ratio of CTA−PEO−CTA to monomer by mass. [b] Determined by GPC calibrated with polystyrene standards. [c] Determined by ^{1}H NMR. The ratio of the integrals of peaks at 5.33 ppm (olefin group in cholesteryl moiety) and 3.64 ppm (PEO repeating unit) is used to calculate the weight fraction of the LC block.

Using this approach, we can obtain amorphous PEO mesostructures at room temperature, which may potentially be used for preparing PEO based lithium ion batteries and other solid-state electrochemical devices.

RESULTS AND DISCUSSION

Synthesis of Monomer, Macromolecular Chain Transfer Agent, and Triblock Copolymers. The synthesis of the triblock copolymer is shown in Scheme 1. A new LC monomer, 5-cholesteryloxypentyl methacrylate (C5MA), is prepared by the esterification of methacryloyl chloride with 5-cholesteryloxypentanol.[57] The composition and purity of C5MA is confirmed by ^{1}H NMR (Supporting Information, Figure S1), GC-MS (Supporting Information, Figure S2), and elemental analysis.

Macromolecular chain transfer agent (CTA−PEO−CTA) is prepared from PEO and the CTA, *S*-1-dodecyl-*S*′-(α,α′-dimethyl-α″-acetic acid)tricarbonate, according to a reported method.[58] To ensure that both ends of the PEO have been modified by CTA, a large excess of CTA in comparison to PEO is used ([CTA]:[PEO] = 5:1). The number-average molecular weight (M_n) of the PEO can be calculated by ^{1}H NMR from the ratio of the integrals of peaks at 3.62 ppm (CH_2CH_2 in PEO repeating unit) and 4.25 ppm (CH_2 of PEO end group connected to CTA moiety) and is found to be 20 394 g/mol (Supporting Information, Figure S3).

The triblock copolymers are prepared by reversible addition−fragmentation chain transfer (RAFT) polymerization. Simply by varying the monomer (C5MA) to CTA−PEO−CTA feed ratio, the molecular weights of the triblock copolymers and the LC weight fractions can be tailored. Here these triblock copolymers with fixed PEO molecular weight (20 kg/mol) and C5MA LC repeating units are referred as TB20-C5MA-Φ, where Φ is the weight fraction of LC block. The ^{1}H NMR spectrum of TB20-C5MA-86 is shown in the Supporting Information, Figure S4. Gel permeation chromatography (GPC) is used to measure the M_n and the polydispersity indices (PDI) of the prepared triblock copolymers, and the results are summarized in Table 1. GPC traces are shown in the Supporting Information, Figure S5.

Thermal Transitions and Nonisothermal PEO Crystallization Behaviors. To identify the thermal transitions in the triblock copolymers, differential scanning calorimetry (DSC) is used. The cooling cycle at a fixed ramping rate is also used to study the nonisothermal PEO crystallization behaviors for the triblock copolymers with different compositions. Figure 1 shows the DSC trace of the TB20-C5MA-60 as an example. The sample is first heated to 250 °C to remove thermal history. In the subsequent first cooling cycle, the isotropic to LC transition is observed at 145.0 °C. The glass transition temperature of PC5MA block ($T_{g,PC5MA}$) and the crystallization temperature of PEO block (T_c) are located at 21.0 and −23.5 °C, respectively. In the second heating cycle, the LC to isotropic transition temperature (T_i) and the glass transition of PEO block ($T_{g,PEO}$) are located at 153.5 and −47.4 °C, respectively, and the melting temperature of PEO (T_m) is observed at 56.7 °C. The transition temperatures and the corresponding transition enthalpies for the homopolymer PC5MA and all the triblock copolymers have been recorded and summarized in Table 2. For TB20-C5MA-21, TB20-C5MA-30, and TB20-C5MA-49, $T_{g,PC5MA}$ cannot be determined because it overlaps with the exothermal peak of PEO crystallization. Specifically, for TB20-C5MA-86, an extra transition peak is observed between T_i and $T_{g,PC5MA}$ in both the heating and cooling cycles (Supporting Information, Figure S6), which is speculated to be a LC to LC transition, and it will be discussed in the next section.

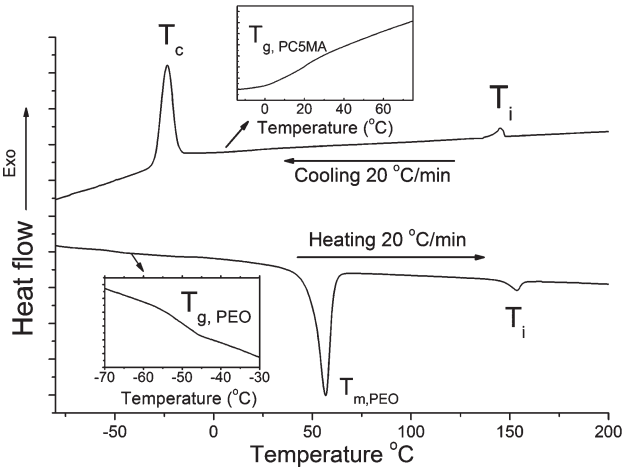

Figure 1. DSC trace of triblock copolymer TB20-C5MA-60.

For triblock copolymers with lower LC contents, TB20-C5MA-21, TB20-C5MA-30, and TB20-C5MA-49, PEO crystallization occurs at the normal undercooling (T_c observed at 31.0−36.4 °C, which is close to that of homopolymer PEO), while for those with higher LC contents, TB20-C5MA-60, TB20-C5MA-72, and TB20-C5MA-86, crystallization occurs at very large undercooling (T_c drops to −23.5 to −27.8 °C) (Table 2). This rapid decline of T_c upon the increasing of LC content is also shown in the stacked DSC traces of the triblock copolymers in the cooling cycle (Figure 2). The stepwise change in the T_c required for the crystallization to occur (different undercooling conditions) suggests different PEO crystallization mechanisms for lower and higher LC content triblock copolymers. From earlier work,[29,32,34,35,37] it is known that this phenomenon is caused by different hierarchical structures at varied LC contents and the nanoconfinement which the hierarchical structures impose on the PEO crystallization. Nevertheless, we notice two interesting features in our triblock copolymers. First, the exceedingly large undercooling for the samples with higher LC contents (TB20-C5MA-60, TB20-C5MA-72, and TB20-C5MA-86) suggest a hard confinement of the PEO crystallization,[32] which

Table 2. Summary of DSC Characterization of CTA−PEO−CTA and Triblock Copolymers[a]

sample	$T_{g,PEO}$/°C[b]	T_c/°C (ΔH/J g^{-1})[c]	$T_{g,PC5MA}$/°C[d]	T_i/°C (ΔH/J g^{-1})[e]	
				heating	cooling
CTA-PEO-CTA	−53.9	37.0 (123.8)	NA	NA	NA
TB20-C5MA-21	−52.2	32.5 (122.9)	NA	NA	NA
TB20-C5MA-30	−53.1	36.4 (112.0)	NA	134.9 (−0.86)	128.5 (0.59)
TB20-C5MA-49	−52.6	31.0 (95.7)	NA	152.9 (−2.58)	144.2 (1.48)
TB20-C5MA-60	−47.4	−23.5 (79.0)	21.0	153.5 (−3.05)	145.0 (1.80)
TB20-C5MA-72	−48.8	−24.5 (66.4)	31.8	164.6 (−3.76)	155.9 (2.91)
TB20-C5MA-86	−48.6	−27.8 (57.8)	31.0	160.3 (−2.66)	153.1 (3.10)

[a] Both the heating and cooling rates are 20 °C/min; samples are first heated to 250 °C to remove thermal history, and all the transitions are recorded in the first cooling or the second heating cycle. [b] Glass transition temperature of PEO block located in the second heating cycle. [c] Crystallization temperature (T_c) and associated enthalpy of PEO block (normalized to the PEO weight fractions) located in the first cooling cycle. [d] Glass transition temperature of the PC5MA block located in the first cooling cycle. [e] LC to isotropic transition temperature (T_i) and associated enthalpy.

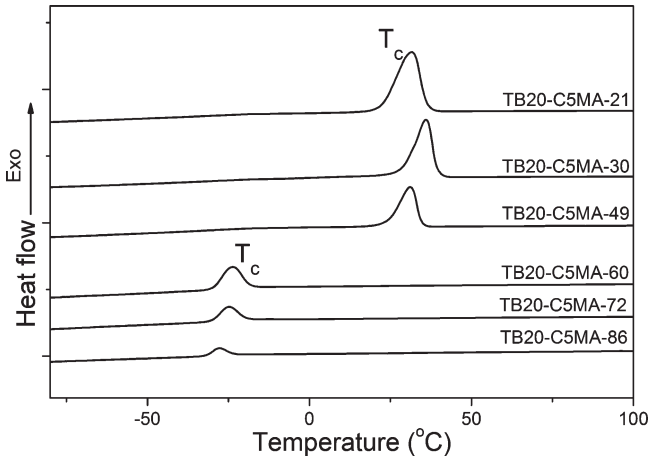

Figure 2. DSC traces of triblock copolymers in the first cooling cycle at a ramping rate of 20 °C/min. The exothermal peaks in the graph are the T_c for the triblock copolymers.

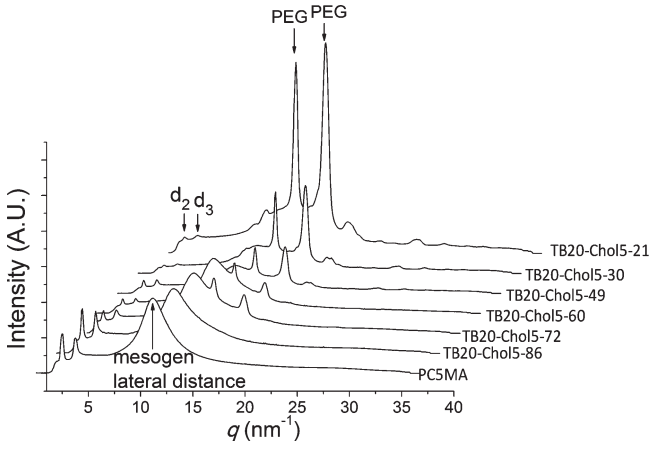

Figure 3. 1D WAXS diffractograms of PC5MA and triblock copolymers at room temperature. The samples are rectangular films prepared by compression molding at 100 °C and subsequently cooled to room temperature in air before testing.

usually happens when T_g of the noncrystalline block is higher than T_m of the crystalline block, while for these samples $T_{g,PC5MA}$ is lower than T_m of PEO. It is inferred that the LC domain, which retains its ordered structure beyond the T_g of the LC block, can provide efficient confinement to the PEO crystallization similar to the confinement effect of the glassy matrix in high-T_g materials. Second, in most published work regarding the frustration of the PEO crystallization by nanoconfinement from BCP microsegregation, the M_n of PEO are limited to less than 10 kg/mol,[34,35,48,49] while the triblock copolymers prepared here has PEO with M_n of 20 kg/mol (determined by NMR), which has a higher melting temperature and crystallization enthalpy compared to the 10 kg/mol samples. Therefore, it is clearly demonstrated that the LC ordering domain can provide efficient confinement to PEO, which leads to suppression of PEO crystallization and even amorphous PEO at room temperature with high LC contents. It should be noticed that the suppression of the PEO crystallization is not at the expense of significantly diluting the PEO content. Even for TB20-C5MA-60 (40 wt % PEO) and TB20-C5MA-72 (28 wt % PEO), exceedingly large undercooling is obtained, as confirmed by DSC.

Analysis of Hierarchical Structures. The hierarchical structures of the triblock copolymers are studied by wide-angle and small-angle X-ray scattering (WAXS and SAXS), which reveals the confinement conditions that the PEO crystallization are subject to, i.e., the geometries of the PEO domains and the structure of the surrounding LC phase. First, 1D WAXS diffractograms of the prepared polymers at room temperature provide the information on their LC ordering (Figure 3). For all the samples, a typical broad halo at q = 11.14 nm^{-1} (d = 0.56 nm) is observed, which is attributed to the lateral distance of the cholesteryl mesogens. Two reflection peaks appear at q = 2.52 and 3.75 nm^{-1} with a ratio of 2:3 and are inferred to be the second- and third-order reflection peaks of smectic ordering. The primary reflection peak is calculated to be q = 1.26 nm^{-1}, matching well with the peak observed at larger angle region in SAXS, which will be discussed later. Using the Braggs' law, the d spacing of the smectic layer (thickness of smectic layer) is found to be 5.0 nm, which is twice the molecular length of the side-chain cholesteryl mesogen with spacer (2.5 nm calculated with ChemBio 3D software). Thus, the LC ordering for the homopolymer and triblock copolymers at room temperature is identified to be bilayer smectic A structure (SmA_2). Specifically, for TB20-C5MA-86 a weak transition is observed between its T_i and $T_{g,PC5MA}$ as determined by DSC. A temperature-controlled WAXS experiment has been conducted, and the transition is

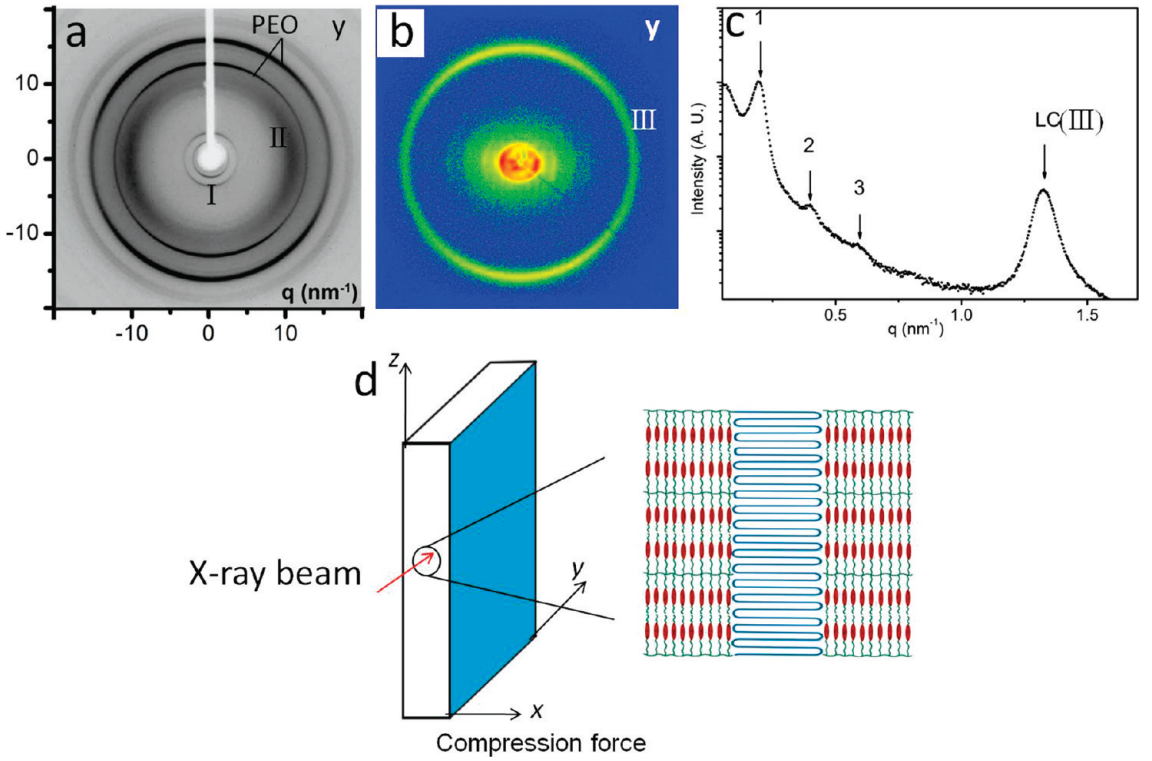

Figure 4. (a) 2D WAXS pattern of TB20-C5MA-49, where (I) indicates the second- and third-order LC reflections and (II) indicates the scattering associated with mesogen lateral distance. (b) 2D SAXS pattern of TB20-C5MA-49, where (III) is the first-order LC reflection peak. (c) 1D SAXS diffractogram of TB20-C5MA-49. (d) Schematic illustration of the hierarchical structure of TB20-C5MA-49 (LC lamellae in PEO lamellae).

identified to be a smectic-to-smectic transition in which the LC packing changes from SmA_2 to slightly interdigitated bilayer (SmA_d) upon heating (see detailed discussion in Supporting Information, Figure S6 and S7).

In the diffractograms of the samples except TB20-C5MA-86 (Figure 3), there are two peaks appearing at q = 13.19 and 15.98 nm^{-1} that are attributed to (120) and mixed ($\bar{1}$32/032) reflections of the PEO crystals, respectively.[59] The intensity of these peaks decreases with increasing LC content. For TB20-C5MA-86 with the highest weight fraction of LC block, the PEO crystallization peaks completely disappear. The decreasing intensity of PEO peaks with the increasing LC content suggests reduction of the PEO crystallinity in the triblock copolymers, which correlates with the trend observed from nonisothermal crystallization experiments by DSC. The complete disappearance of the PEO crystallization peaks at room temperature in TB20-C5MA-86 confirms that amorphous PEO material is obtained at room temperature.

The combination of 2D WAXS and SAXS is used to analyze the hierarchical structures present in the triblock copolymers and the anchoring condition of the mesogens to the intermaterials dividing surface (IMDS) in the polymer films prepared by compression molding. First we investigate TB20-C5MA-49 as an example of triblock copolymers with lower LC contents and higher T_c. Figure 4a shows the 2D WAXS pattern of TB20-C5MA-49. X-ray beam is set perpendicular to the edge of the film because the diffraction pattern for the face of the film does not give enough orientation information for analysis (Supporting Information, Figure S8). Two reflections bands at small angles (I) are due to the second- and third-order LC peaks, respectively, as also located in the 1D diffractogram in Figure 3. A broad scattering at larger angle (II) is associated with the lateral distance of the cholesteryl mesogens. The LC reflections (I) are stronger along the meridian direction while the lateral distance scattering (II) is stronger along the equator direction. The observed orthogonality (also shown in the azimuthal plot in Supporting Information, Figure S8g) is typical of smectic A structure, in which the mesogens are arranged perpendicular to the smectic layer.[43,52,60,61] The two sharp reflection bands in the wide-angle region due to PEO crystallization appear to be parallel to the LC reflection, implying that the PEO crystal (c-axis) is parallel to the smectic layer.[59] The BCP microphase separation structure of the TB20-C5MA-49 is identified by 2D SAXS (Figure 4b). In the converted 1D SAXS diffractogram (Figure 4c), scattering peaks with a q-relationship of 1:2:3 are recorded, showing a lamellar structure. The d spacing of the lamellar structure is calculated to be 35 nm from the primary reflection peak q_1 = 0.18 nm^{-1}. The reflection (III) with the peak value of q = 1.28 nm^{-1} is the first-order peak of the smectic layer diffraction, which is commensurate reasonably with the higher ordered LC peaks observed by WAXS. From the anisotropic rings in the 2D SAXS image (Figure 4b), it can be seen that the LC reflection band (III) is stronger at the meridian direction while the microphase separation reflections are stronger at the equator direction, proving that the smectic layers are perpendicular to the block copolymer microphase-separated lamellae. Combining the information from both 2D WAXS and SAXS patterns, the hierarchical structure of TB20-C5MA-49 can be determined to be a "LC lamellae in PEO lamellae" structure, in which the smectic layers are perpendicular to the microphase separated lamellae and the cholesteryl mesogens align parallel to the IMDS (homogeneous anchoring) (Figure 4d).

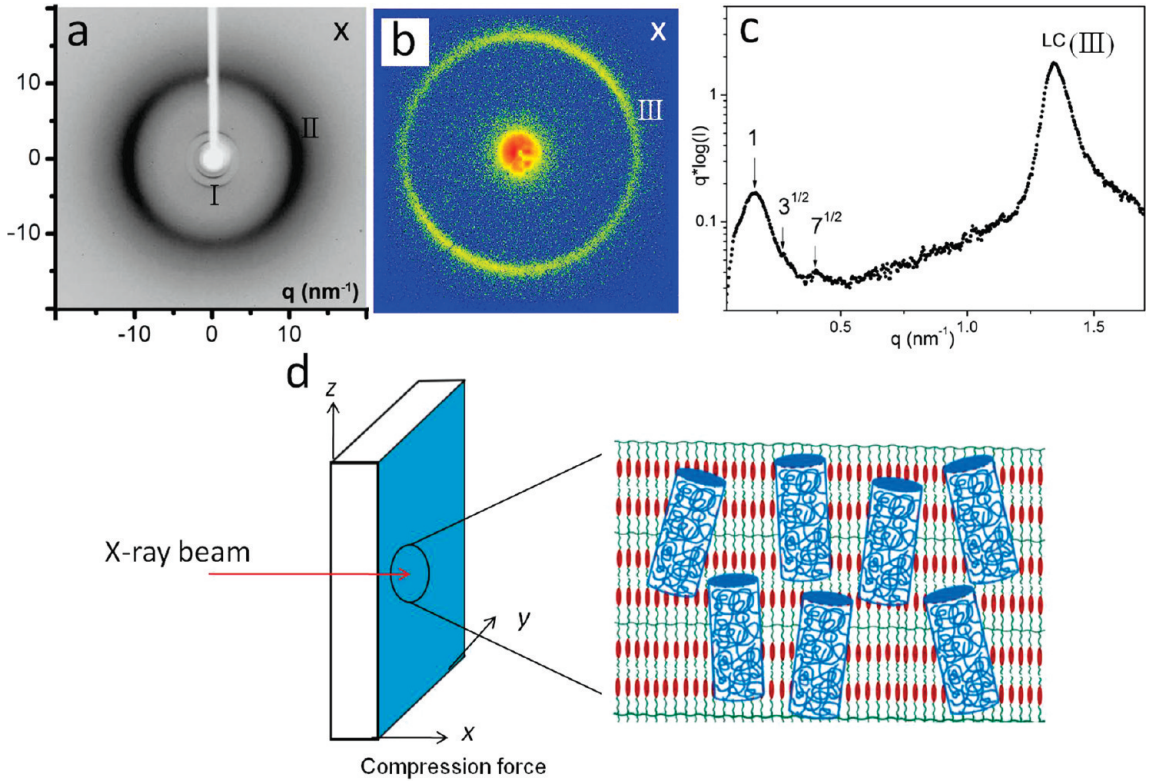

Figure 5. (a) 2D WAXS pattern of TB20-C5MA-86, where (I) indicates the second- and third-order LC reflections and (II) indicates the scattering associated with mesogen lateral distance. (b) 2D SAXS pattern of TB20-C5MA-86, where (III) is the first-order LC reflection peak. (c) 1D SAXS diffractogram of TB20-C5MA-86. (d) Schematic illustration of the hierarchical structure of TB20-C5MA-86 (PEO cylinders in LC matrix).

Similar "lamellae in lamellae" structures of cholesterol-based LC phase within microsegregated lamellae have been reported by Ikkala et al., in which the cholesteryl mesogens are connected to block copolymer backbone through covalent, hydrogen, or ionic bonding.[62−64]

For samples with higher LC contents where large undercooling is required for PEO crystallization, we study TB20-C5MA-86 as an example. The X-ray beam is incident along the normal of the face of the film because the diffraction pattern for the edge of the film does not give enough orientation information for analysis (Supporting Information, Figure S9). In the 2D WAXS image of TB20-C5MA-86 (Figure 5a), the orthogonality of the second- and third-order LC reflection bands (I) and the lateral distance scattering (II) have been observed, indicating the smectic A structure. PEO crystallization rings are not observed, proving the lack of crystallization in this sample. In the 1D diffractogram of TB20-C5MA-86 (Figure 5c), primary peak and weakly intense higher order peaks ($\sqrt{3}$ and $\sqrt{7}$) are observed. The *d* spacings of the microsegregation domains are calculated to be 52 nm from the primary reflection peak at 0.12 nm^{-1}. The lack of distinct higher order reflections possibly suggests a cylindrical morphology with poor long-range ordering. This is also observed in the 2D SAXS pattern (Figure 5b), and therefore, anchoring condition of the LC mesogens with respect to the IMDS cannot be inferred. Combining the results from WAXS and SAXS, we conclude that the sample TB20-C5MA-86 possesses a "PEO cylinders in LC matrix" structure, in which amorphous PEO cylinders are dispersed in the LC matrix as illustrated in Figure 5d. Similar "cylinders in LC lamellae" structures with cylinders in a well-ordered hexagonal symmetry have been previously reported.[65,66] Compared to these, the current triblock copolymer does not exhibit long-range ordering of the PEO cylinders. This is possibly associated with the large molecular weight of TB20-C5MA-86, which leads to the limited chain diffusion and mobility and consequently strong kinetic resistance to form long-range periodic mesostructures.[9,67−69]

SAXS experiments have also been performed for TB20-C5MA-21, TB20-C5MA-30, TB20-C5MA-60, and TB20-C5MA-72 to identify their microphase-separated structures, and the results are shown in the 1D diffractograms in Figure 6. For TB20-C5MA-21, only the primary peak at $q = 0.25$ nm^{-1} is recorded. The lack of higher order peaks suggests the "breakout" of PEO crystals, forming a 3D continuous crystallization phase which disrupts the microphase separation structure.[35] For TB20-C5MA-30, a "LC lamellae in PEO lamellae" structure is identified from peaks with *q*-relationship of 1:2:3, and for TB20-C5MA-60 a "PEO cylinders in LC matrix" structure is identified from *q*-relationship of $1:\sqrt{3}:\sqrt{7}$. For TB20-C5MA-72, a primary peak and a shoulder peak with *q*-relationship of $1:\sqrt{3}$ have been observed, suggesting a cylindrical morphology albeit with poor ordering.

Transmission electron microscopy (TEM) experiments of the ultrathin sections of the samples are performed to confirm the morphologies of the prepared triblock copolymers. Figure 7a shows the lamellar structure of TB20-C5MA-49, in which the PEO domains are more preferentially stained and appear as darker regions. The *d* spacing of the lamellar structure measured from the TEM image is 27 nm, which is lower than that from SAXS, likely due to the shrinkage of the sample during the freeze-drying process after the cryo-microtoming and/or the TEM

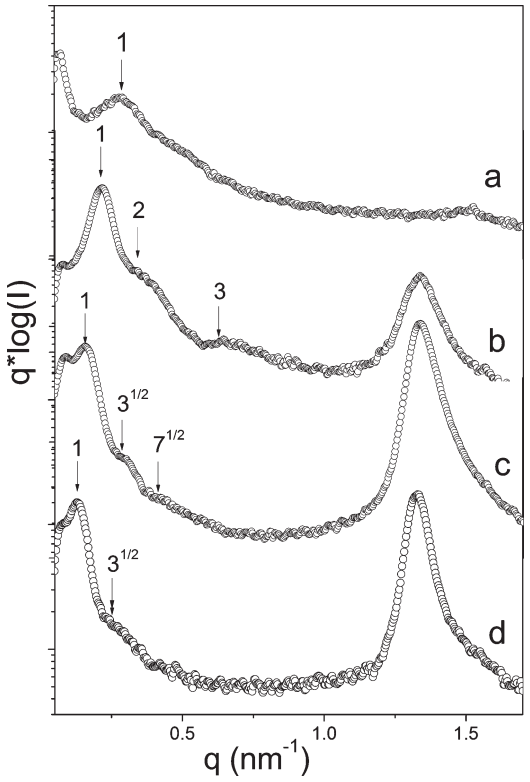

Figure 6. 1D SAXS diffractograms of (a) TB20-C5MA-21 (disrupted microsegregated structure), (b) TB20-C5MA-30 with a lamellar structure (LC lamellae in PEO lamellae), (c) TB20-C5MA-60 with a cylindrical structure (PEO cylinders in LC matrix), and (d) TB20-C5MA-72 with a cylindrical structure (PEO cylinders in LC matrix).

viewing angle.[10] The TEM images of TB20-C5MA-86 (Figure 7b,c) show both circular and rodlike concentrations of electron density, which are attributed to the top and side views of PEO cylinders, respectively. The irregularity of the circular spots and rods is due to the fact that this sample does not exhibit long-range order. This TEM data agree with the SAXS of TB20-C5MA-86, in which only primary peak and weak intensity increase at $\sqrt{3}$ and $\sqrt{7}$ are observed. It is noticed that the peripheries of the cylinders appear darker than other regions (Figure 7b,c). The reason is unclear but possibly due to the staining artifact caused by the diffusion gradient at the domain boundaries. Since the polymer does not exhibit long-range order or hexagonal packing, the domain spacing has not been estimated from TEM for comparison with SAXS result. The cylindrical morphology of TB20-C5MA-72 has also been confirmed by TEM (Supporting Information, Figure S10), in which both circular and rodlike features can be observed, showing the top and side views of PEO cylinders, respectively.

In Table 3, we summarize the hierarchical structure information including the LC ordering along with the microsegregated morphologies for the triblock copolymers. TB20-C5MA-21 possesses a disrupted microsegregated structure with "breakout" or unconfined PEO crystallization domain, while TB20-C5MA-30 and TB20-C5MA-49 both have lamellar structures. Thus, for all the samples with normal undercooling conditions for crystallization, PEO crystallization occurs in more continuous phase (3D matrix or 2D lamellae). In contrast, for TB20-C5MA-60, TB20-C5MA-72, and TB20-C5MA-86 which require large undercooling for crystallization, the BCP microsegregated structures are found to be "PEO cylinders in LC matrix"; thus, PEO crystallization is confined within more isolated cylindrical domains. Similar results as to the influence of different microsegregated nanostructures on PEO crystallization have been reported previously.[28−32,34] Here by varying the LC contents, we are able to tailor the hierarchical structures of the polymers, which provide different confinements to PEO and thus lead to altered crystallization behaviors. The "PEO cylinders in LC matrix" structures are observed at 40−14 wt % of PEO (60−86 wt % of LC block), which deviates from the phase diagram of conventional coil−coil block copolymers.[70,71] This is probably due to the structural and conformational asymmetry caused by the LC block and the anchoring of LC mesogens to the IMDS which impact the microphase separation[39] and the possible interaction of the two LC end blocks of the triblock copolymers which results in a modified phase diagram, in contrast to that of conventional coil−coil diblock copolymers.[72]

Impact of Hierarchical Structures on the PEO Crystallization. The structure analysis by WAXS and SAXS reveals that by varying the LC content hierarchical structures of the triblock copolymers can be tailored, leading to unconfined or nanoconfined PEO, i.e., 3D continuous network, 2D lamellae in lamellae, and 1D cylinders.[34] To further investigate the PEO crystallization mechanism in different confining environments, isothermal crystallization experiments and Avrami analysis are conducted. TB20-C5MA-49 and TB20-C5MA-86 are studied as representatives for "LC lamellae in PEO lamellae" and "PEO cylinders in LC matrix", respectively. TB20-C5MA-21 with "LC cylinders in PEO matrix" structure is not further studied, since in this case PEO can crystallize over a macroscopic length scale in 3D continuous phase similar to PEO homopolymer.[34] In Avrami analysis, isothermal crystallization of the polymer is performed and the normalized crystallinity $X_c(t)$ at time t is recorded, which can be fitted to the Avrami equation

$$X_c(t) = 1 - \exp(-kt^n)$$

where k is the crystallization rate constant and n is the Avrami exponent. The Avrami exponent n depends on the crystallization mechanism and the nanodomain geometry in which the crystal grows.[34,35,37,73] In microstructures such as spherical or cylindrical morphologies, crystallization is confined within more isolated microdomains, in which usually only one nucleus is formed in a single microdomain. Thus, the crystallization is initiated through homogeneous nucleation mechanism, and the subsequent crystal growth is completed very quickly because the long-range crystal growth is frustrated by the matrix of the noncrystalline block surrounding the microdomains.[28,34,35,37] As a result, the crystallization kinetics is dominated by the homogeneous nucleation, providing a simple exponential relationship between X_c and t, and n is around 1.[28,34,35,37] Since the energy barrier for homogeneous nucleation is much larger compared to that of heterogeneous nucleation, large undercooling (T_c much lower than T_m) is usually necessary to initiate crystallization.[34,36,37,74] For crystallization confined in more continuous microdomains such as lamellar structures, in which the crystals can grow in 2D spaces, heterogeneous nucleation occurs more easily and long-range crystal growth is possible in continuous microdomains. Therefore, the crystallization kinetics is determined by both the nucleation rate and the subsequent crystal growth rate, and n is usually larger than one ($\sim$2).[30−32,34,37,73] In this case, normal undercooling (T_c close to T_m) is sufficient to initiate the heterogeneous nucleation.

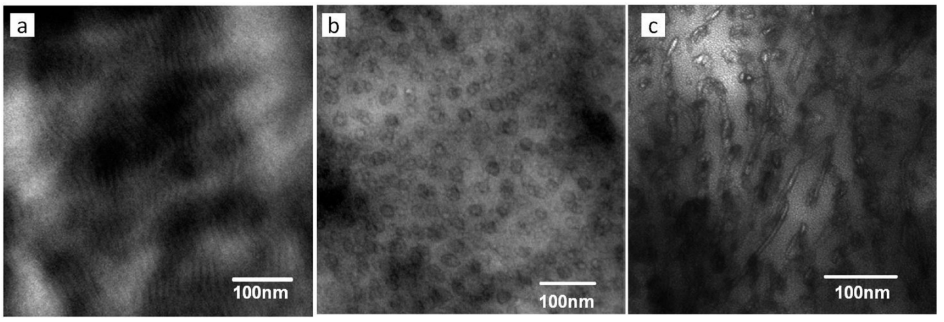

Figure 7. TEM micrographs of (a) TB20-C5MA-49, (b) TB20-C5MA-86 (top view of cylinders) and (c) TB20-C5MA-86 (side view of cylinders). The samples are stained with RuO_4 and PEO domains appear as darker regions.

Table 3. Summary of the Hierarchical Structure Information for the Triblock Copolymers

		microphase separation		
sample	LC ordering	q_1 (nm^{-1})	d spacing (nm)	hierarchical structure
TB20-C5MA-21	SmA_2	0.25	25	disrupted microstructure
TB20-C5MA-30	SmA_2	0.21	30	LC lamellae in PEO lamellae
TB20-C5MA-49	SmA_2	0.18	35	LC lamellae in PEO lamellae
TB20-C5MA-60	SmA_2	0.16	39	PEO cylinders in LC matrix
TB20-C5MA-72	SmA_2	0.13	48	PEO cylinders in LC matrix
TB20-C5MA-86	SmA_2	0.12	52	PEO cylinders in LC matrix

From our Avrami experiments, it is found that the Avrami exponent n for TB20-C5MA-49 is 1.5−1.7 (Figure 8a). Since TB20-C5MA-49 has a "LC lamellae in PEO lamellae" structure, the $n \approx 2$ suggests 2D crystal growth mechanism confined in PEO lamellar domains.[37,73] Considering the fact that TB20-C5MA-49 crystallizes at normal undercooling, we can thus infer the crystallization mechanism of this sample to be heterogeneous nucleation followed by 2D crystal growth confined between LC walls. In contrast, the Avrami exponent n for TB20-C5MA-86 is found to be around 1.1 (Figure 8b). This value is close to 1, the simple exponential relation between X_c and t_c suggests that the PEO crystallization is dominated by homogeneous nucleation.[34] Since TB20-C5MA-86 has a "PEO cylinders in LC matrix" microstructure, we can conclude that the PEO crystallization in this case follows a homogeneous nucleation mechanism and long-range crystal growth is prohibited by the LC matrix surrounding the cylindrical microdomains. Therefore, the crystallization is strongly reduced, and much larger undercooling is required to initiate crystallization.

Given the relatively small n values found by the Avrami analysis, it is demonstrated that efficient confinement of crystallization can be provided by LC domains for both the higher and lower LC content triblock copolymers. This is likely due to the following aspects (1) the presence of the LC phase may increase the incompatibility of the two polymer blocks, which can enhance

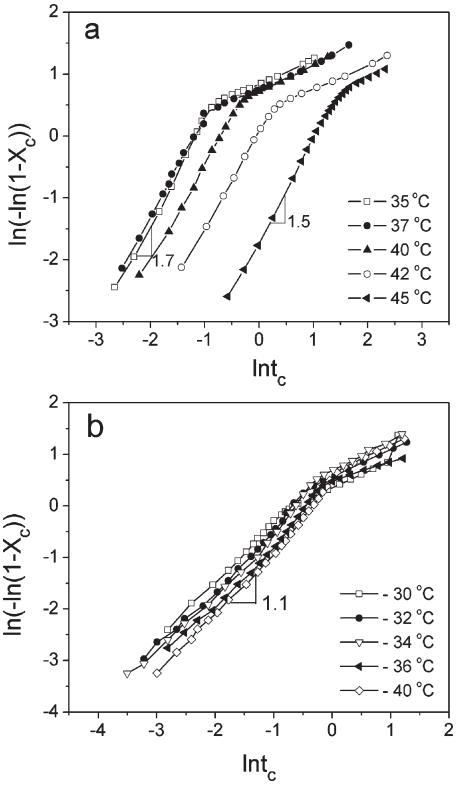

Figure 8. Avrami plots for (a) TB20-C5MA-49 with "LC lamellae in PEO lamellae" structure and (b) TB20-C5MA-86 with "PEO cylinders in LC matrix" structure.

the microphase separation, (2) the preformed LC ordering needs to be disrupted to allow long-range crystal growth, which may require additional energy, and (3) high viscosity of the LC domain prevents the crystallization to propagate through the spatial discontinuity caused by microphase separation. However, more investigations including determination of the χ parameters of the prepared block copolymers are required to verify these speculations. Also, by increasing the LC content, the resulting "PEO cylinders in LC matrix" leads to homogeneous nucleation dominated crystallization and exceedingly large undercooling for crystallization. This result correlates well with the WAXS experiment of TB20-C5MA-86, in which PEO crystalline reflection peaks completely disappeared at room temperature. Therefore, without adding any dopants or additives, we can successfully obtain amorphous PEO of 20 kg/mol molecular weight at room

temperature simply by increasing the LC content in the block copolymers.

CONCLUSION

In the present study, a series of LC−semicrystalline−LC triblock copolymers have been prepared using the RAFT method. By varying the LC content in the triblock copolymers, different hierarchical structures including "LC lamellae in PEO lamellae" and "PEO cylinders in LC matrix" have been obtained. It is observed that the nanoconfinement resulting from different hierarchical structures at varied LC contents strongly influences the PEO crystallization behavior. For triblock copolymers with lower LC contents and "LC lamellae in PEO lamellae", PEO crystallization is subject to 1D confinement by the LC domains, and the crystallization is initiated by heterogeneous nucleation followed by long-range crystal growth in 2D microdomains. Thus, normal undercooling is sufficient for crystallization to occur (T_c = 31.0−36.4 °C). For polymers with higher LC content and "PEO cylinders in LC matrix", PEO crystallization is confined within isolated cylindrical domains. Thus, homogeneous nucleation dominates with long-range crystal growth hindered by the LC matrix, resulting in the frustration of PEO crystallization and much larger undercooling (T_c = −23.5 to −27.8 °C). Since the microsegregated LC domain can efficiently confine the crystallization, this study provides a practical method of exploiting hierarchical structures to tailor the PEO crystallization behavior. Using this simple approach, we can obtain amorphous nanostructures of PEO at room temperature, which can potentially be used for preparing PEO based lithium ion batteries and other solid-state electrochemical devices. In the future, by tweaking the molecular weight, the composition as well as the functionality of these LC-PEO BCPs, long-range ordered amorphous PEO domains may be obtained by aligning the LC mesophase with magnetic field.[12,13,42,52,55,56]

EXPERIMENTAL SECTION

Materials. 2,2-Azobis(2-methylpropionitrile) (AIBN, Sigma-Aldrich, 98%), cholesterol (Alfa Aesar, 96%), methacryloyl chloride (Fluka, >97%), 1,5-pentanediol (Fluka, >97%), *p*-toluenesulfonyl chloride (tosyl chloride, Sigma-Aldrich, 99%), poly(ethylene oxide) 20 000 (M_n = 20 kg/mol, Fisher), tetrahydrofuran (THF, Sigma-Aldrich, anhydrous, >99.9%), 1,4-dioxane (Acros, 99.8%, extra dry), dichloromethane (Acros, 99.9%, extra dry), and triethylamine (Sigma-Aldrich, >99%) were used as received. *S*-1-Dodecyl-*S*′-(α,α′-dimethyl-α′′-acetic acid)-tricarbonate, a RAFT chain transfer agent (CTA), is synthesized according to the procedure described by Lai et al.[75]

Synthesis of Monomer, C5MA. LC monomer 5-cholesteryloxypentyl methacrylate (C5MA) is prepared as illustrated in Scheme 1. The detailed procedure is described as below.

Cholestryl Tosylate, ***1***. Cholestryl tosylate is prepared from tosyl chloride and cholesterol according to a published procedure.[76] ^{1}H NMR ($CDCl_3$, δ ppm): 7.80, 7.34 (4H, aromatic), 5.30 (d, 1H, −C═C*H*−, olefin group in cholesteryl moiety), 4.32 (m, 1H, $-SO_2-OCH-$), 2.45 (s, 3H, CH_3 in tosyl group), 2.50−0.55 (m, 43H, $-CH_3$, $-CH_2-$, −C*H*−, −C*H*(CH_3)− in cholesteryl moiety). IR (KBr pellet, cm^{-1}): 2700−3100 (alkene and alkane C−H stretching), 1603 (aromatic C═C), 1356 (S═O).

5-Cholesteryloxypentanol, ***2***. Cholesteryl tosylate (10.0 g, 18.5 mmol) and 1,5-pentanediol (9.6 g, 92.4 mmol) are refluxed in 150 mL of 1, 4-dioxane for 20 h. Afterward, the solution is concentrated and redissolved in 100 mL of dichloromethane, followed by washing with 3 × 100 mL of deionized water. The dichloromethane layer is collected and concentrated and then recrystallized from cold acetone. The solid product is collected and dried *in vacuo* (light yellow solid, yield 58%). ^{1}H NMR ($CDCl_3$, δ ppm): 5.34 (d, 1H, −C═C*H*−, olefin group in cholesteryl moiety), 3.64 (t, 2H, $-CH_2OH$), 3.45 (t, 2H, $-CH_2OCH-$), 3.12 (m, 1H, $-CH_2OCH-$), 2.50−0.55 (m, 49H, $-CH_3$, $-CH_2-$, −C*H*−, −C*H*(CH_3)− in cholesteryl moiety, $-CH_2CH_2CH_2CH_2CH_2-$ in spacer). IR (KBr pellet, cm^{-1}): 3300−3700 (−OH), 2700−3100 (alkene and alkane C−H stretching), 1639 (C═C), 1130 (C−O−C).

5-Cholesteryloxypentyl Methacrylate (C5MA), ***3***. 5-Cholesteryloxypentanol (5.0 g, 10.6 mmol) and 25 mL of triethylamine are dissolved in 50 mL of THF and refluxed. To the refluxing solution, methacryloyl chloride (4.8 g, 46.0 mmol) is added in a dropwise fashion. The reaction mixture is further refluxed for 20 h. The insoluble ammonium salt is removed by filtration. The filtrate is concentrated and redissolved in dichloromethane and then washed with 3 × 100 mL of HCl aqueous solution (1.6 N). The dichloromethane layer is collected and precipitated in methanol. The crude product is further purified by column chromatography (silica gel, dichloromethane). The purity of the final product has also been confirmed by thin layer chromatography, showing a single spot on the plate (colorless viscous liquid product, yield 37%). ^{1}H NMR ($CDCl_3$, δ ppm): 6.09, 5.54 (m, 2H, CH_2═C(CH_3)COO−), 5.33 (d, 1H, −C═C*H*−, olefin group in cholesteryl moiety), 4.15 (t, 2H, $-COOCH_2-$), 3.46 (t, 2H, $-CH_2OCH-$), 3.11 (m, 1H, $-CH_2-OCH-$), 2.50−0.55 (m, 52H, $-CH_3$, $-CH_2-$, −C*H*−, −C*H*(CH_3)− in cholesteryl moiety, CH_2═C(CH_3)COO−, $-CH_2CH_2CH_2CH_2CH_2-$ in spacer). IR (KBr pellet, cm^{-1}): 2700−3100 (alkene and alkane C−H stretching), 1720 (C═O), 1639 (C═C), 1130 (C−O−C). GC-MS (*m*/*z*): 540.60 (M), Calcd: 540.45. Anal. Calcd for $C_{36}H_{60}O_3$: C, 79.94; H, 11.18. Found: C, 79.66; H, 11.19.

Synthesis of Homopolymer, PC5MA. Monomer C5MA (0.5 g, 0.93 mmol) is dissolved in 4 mL of 1,4-dioxane in a Schlenk tube equipped with a stir bar, followed by the addition of the CTA, *S*-1-dodecyl-*S*′-(α,α′-dimethyl-α′′-acetic acid)tricarbonate (18.3 mg, 0.05 mmol), and the initiator, AIBN (0.82 mg, 0.005 mmol). The Schlenk tube is degassed by three freeze−pump−thaw cycles and then placed in a 75 °C oil bath. The reaction is allowed to proceed for 20 h. The reaction mixture is concentrated and precipitated in acetone. The product polymer is collected and dried *in vacuo* (light yellow solid, yield 75%). ^{1}H NMR ($CDCl_3$, δ ppm): 5.33 (d, 1H, −C═C*H*−, olefin group in cholesteryl moiety), 3.92 (m, 2H, $-COOCH_2CH_2-$), 3.45 (m, 2H, $-CH_2OCH-$), 3.12 (m, 1H, $-CH_2OCH-$), 2.50−0.55 (m, 54H, $-CH_3$, $-CH_2-$, −C*H*−, −C*H*(CH_3)− in cholesteryl moiety, $-CH_2-C(CH_3)COO-$, $-CH_2CH_2CH_2CH_2CH_2-$ in spacer). GPC (40 °C, THF mobile phase, polystyrene standards): M_n = 13 964 g/mol, PDI = 1.19.

Synthesis of Macromolecular Chain Transfer Agent, CTA−PEO−CTA. The macromolecular chain transfer agent CTA−PEO−CTA is prepared according to a modified reported procedure.[58] CTA *S*-1-dodecyl-*S*′-(α,α′-dimethyl-α′′-acetic acid)tricarbonate (0.475 g, 1.3 mmol) is dissolved in 25 mL of dichloromethane in an air-free flask sealed with a rubber septum and connected to a bubbler. The flask is purged with N_2 for 20 min, after which oxalyl chloride (0.55 mL, 6.4 mmol) is injected into the flask over 15 min. The mixture is stirred under N_2 atmosphere for about 2 h until the gas evolution stops. The volatiles are then removed under vacuum. The flask is again purged with N_2 and PEO 20 000 (5 g in 40 mL of dichloromethane) is added through a cannula. The reaction is allowed to proceed for 24 h. The product is precipitated in *n*-hexane and washed numerous times with *n*-hexane to remove unreacted CTA and finally dried *in vacuo* at room temperature (light yellow powder, yield 95%.) ^{1}H NMR ($CDCl_3$, δ ppm): 4.25 (t, 2H, $-COOCH_2-$ in PEO end group), 3.62 (m, $-CH_2CH_2O-$, repeating units of PEO), 3.25 (t, 2H, $CH_3C_{10}H_{20}CH_2-S-$), 1.50−1.75 (m, 6H, $-S-C(CH_3)_2COO-$), 1.25 (m, 20H, $CH_3C_{10}H_{20}CH_2S-$),

0.87 (t, 3H, $CH_3C_{10}H_{20}CH_2S-$). M_n = 20 394 g/mol (calculated from ^{1}H NMR by the ratio of peaks at 3.62 and 4.25 ppm). GPC (40 °C, THF mobile phase, polystyrene standards): M_n = 15 059 g/mol, PDI = 1.06.

Synthesis of Triblock Copolymer, TB20-C5MA-Φ. Triblock copolymers TB20-C5MA-Φ with different weight fractions of LC block have been prepared using RAFT polymerization, as illustrated in Scheme 1. In a representative procedure of synthesizing TB20-C5MA-86, AIBN (0.46 mg, 0.0028 mmol), CTA-PEO-CTA (0.25 g, 0.0125 mmol), and C5MA (1.5 g, 2.78 mmol) are dissolved in 5 mL of 1, 4-dioxane in a Schlenk tube equipped with a stir bar. The Schlenk tube is degassed by three freeze−pump−thaw cycles and placed in a 75 °C oil bath. The reaction is allowed to proceed for 20 h. The reaction mixture is concentrated and precipitated in diethyl ether. The product polymer is collected and dried *in vacuo* (light yellow solid, yield 58%) ^{1}H NMR ($CDCl_3$, δ ppm): 5.33 (d, 1H, −C═C*H*−, olefin group in cholesteryl moiety), 3.92 (m, 2H, −COOCH_2CH$_2$−), 3.64 (m, −CH_2CH_2O− repeating units of PEO), 3.45 (m, 2H, −CH_2OCH−), 3.12 (m, 1H, −CH$_2$OC*H*−), 2.50−0.55 (m, 54H, −CH_3, −CH_2−, −C*H*−, −C*H*-(CH_3)− in cholesteryl moiety, −CH_2−C(CH_3)COO−, −CH$_2$CH_2-CH_2CH_2CH$_2$− in spacer). GPC (40 °C, THF mobile phase, polystyrene standards): M_n = 56 060 g/mol, PDI = 1.40.

Instrumental Procedures. ^{1}H NMR is recorded on a Bruker DMX500 high-resolution digital NMR spectrometer. Fourier transform infrared spectroscopy (FTIR) of the samples as KBr pellets were tested on a Nicolet Magna-IR 560 spectrometer. Elemental analysis is carried out using a Vario MICRO Elementar, calibrated with sulfanilamide standard, which simultaneously detects C, H, N, and S percentage. Gas chromatography−mass spectrometry (GC-MS) is performed with Hewlett-Packard 5890 and 6890 Series gas chromatography mass spectrometer. The number-average molecular weight (M_n) and polydispersity indices (PDI) of the polymers are determined by gel permeation chromatography (GPC) using a Waters 150-C ALC/GPC equipped with evaporative light scattering detector. THF is used as the eluent with a flow rate of 2.0 mL/min at 40 °C. Polystyrene is used as standard.

Thermal Transitions and Isothermal Crystallization Experiment. The phase transitions of the triblock copolymers are studied by differential scanning calorimetry (DSC) on TA Instruments DSC Q-20 series. The powder sample is kept in a hermetically sealed alumina pan with another empty pan as reference. Both heating and cooling cycles are carried out at a ramping rate 20 °C/min.

The isothermal crystallization experiment has been performed with DSC to study PEO crystallization mechanism and kinetics.[35,37] To avoid possible thermal lag, only ∼1 mg sample is used. The sample is kept in a hermetically sealed alumina pan and heated up to 75 °C and equilibrated for 10 min to melt the PEO crystals. Subsequently, the sample is quenched to the desired crystallization temperature at a rate of 100 °C/min and kept isothermal for 35−50 min to ensure the completion of crystallization, during which the heat flow versus the time is recorded. Subsequently, the sample is reheated to 75 °C at a rate of 5 °C/min, and the melting temperature (T_m) and the enthalpy (ΔH) are recorded.

Microstructure Analysis. 2D WAXS has been used to investigate the liquid crystalline properties as well as the PEO crystallization of the triblock copolymers. The experiment is performed on Oxford diffraction Xcalibur PX Ultra with X-ray beam of CuKα radiation (λ = 1.54 Å) and an Onyx CCD detector which covers the range of 2.8°−51.1°. Rectangular samples are prepared by compression molding of powdered samples at 100 °C and subsequently cooled to room temperature in the air. X-ray beam is aligned along the normal to the face or the edge of the film to obtain the orientation information.

2D SAXS experiments are used to study the microphase separation structures of the triblock copolymers. The samples prepared by compression molding are further annealed at around 170 °C *in vacuo* for 24 h to enhance the ordering of microphase separation. X-ray beam (λ = 1.54 Å) is produced by a Cu Kα microsource (Rigaku). Silver behenate is used for calibration, which has a lamellar structure with *d* spacing of 58.38 Å. The scattering pattern is recorded on a gas-filled wire array detector (Molecular Metrology, Inc.) with a distance of about 150 cm from the sample, providing an accessible angular range corresponding to dimensions between about 4 and 100 nm.

TEM study is performed on Tecnai Biotwin G2 TEM with accelerating voltage of 80 kV. Thin sections with ∼100 nm thickness are obtained using a Leica Ultracut UCT microtome with a glass knife at −80 °C and then slowly brought back to room temperature through a freeze-dry process to avoid the absorption of moisture. The thin sections are collected onto 100 mesh TEM grids covered by carbon-coated Formvar film and stained in RuO_4 vapor at room temperature for 30 min.

■ ASSOCIATED CONTENT

Supporting Information. Figures showing ^{1}H NMR spectra of C5MA, CTA−PEO−CTA, and TB20-C5MA-86, a mass spectrum of C5MA, DSC trace and temperature controlled X-ray diffractograms of TB20-C5MA-86, 2D WAXS patterns for all the triblock copolymers, TEM image and AFM phase contrast image of TB20-C5MA-72, etc. This material is available free of charge via the Internet at http://pubs.acs.org.

■ AUTHOR INFORMATION

Corresponding Author
*E-mail: Kasi@ims.uconn.edu.

■ ACKNOWLEDGMENT

Financial support was provided by the University of Connecticut new-faculty start-up fund, University of Connecticut Research Foundation faculty grant, NSF CAREER Award to R.M.K. (DMR-0748398). Chinedum O. Osuji and Manesh Gopinadhan acknowledge financial support from NSF under DMR-0847534. Central instrumentation facilities in the Institute of Materials Science and Chemistry Department and transmission electron microscopy facility in the Physiology and Neurobiology Department at University of Connecticut are acknowledged. The authors are very thankful to the NSF-MRSEC X-ray Scattering Laboratory at University of Massachusetts Amherst for using their Rigaku-Molmet SAXS-WAXS equipment for our SAXS data collection and Dr. Dhanasekaran Thirunavukkarasu for helpful assistance and covering the user fee through a NSF-MRSEC Materials Research Facilities Network grant. The authors also thank Stephen Daniels for performing cryomicrotomy sectioning and TEM experiments of the samples. The authors are grateful for insightful comments and feedback from the reviewers.

■ REFERENCES

(1) Gadjourova, Z.; Andreev, Y. G.; Tunstall, D. P.; Bruce, P. G. *Nature* **2001**, *412*, 520–523.
(2) MacGlashan, G. S.; Andreev, Y. G.; Bruce, P. G. *Nature* **1999**, *398*, 792–794.
(3) Staunton, E.; Andreev, Y. G.; Bruce, P. G. *Faraday Discuss.* **2007**, *134*, 143–156.
(4) Druger, S.; Ratner, M.; Nitzan, A. *Solid State Ionics* **1983**, *9*, 1115–1120.
(5) Angell, C.; Liu, C.; Sanchez, E. *Nature* **1993**, *362*, 137–139.
(6) Cho, B.-K.; Jain, A.; Gruner, S. M.; Wiesner, U. *Science* **2004**, *305*, 1598–1601.
(7) Kim, S. H.; Misner, M. J.; Yang, L.; Gang, O.; Ocko, B. M.; Russell, T. P. *Macromolecules* **2006**, *39*, 8473–8479.

(8) Munch Elmér, A.; Jannasch, P. *Solid State Ionics* **2006**, *177*, 573–579.
(9) Singh, M.; Odusanya, O.; Wilmes, G. M.; Eitouni, H. B.; Gomez, E. D.; Patel, A. J.; Chen, V. L.; Park, M. J.; Fragouli, P.; Iatrou, H.; Hadjichristidis, N.; Cookson, D.; Balsara, N. P. *Macromolecules* **2007**, *40*, 4578–4585.
(10) Young, W.-S.; Brigandi, P. J.; Epps, T. H. *Macromolecules* **2008**, *41*, 6276–6279.
(11) Young, W.-S.; Epps, T. H. *Macromolecules* **2009**, *42*, 2672–2678.
(12) Gopinadhan, M.; Majewski, P. W.; Osuji, C. O. *Macromolecules* **2010**, *43*, 3286–3293.
(13) Majewski, P. W.; Gopinadhan, M.; Jang, W.-S.; Lutkenhaus, J. L.; Osuji, C. O. *J. Am. Chem. Soc.* **2010**, *132*, 17516–17522.
(14) Tirumala, V. R.; Romang, A.; Agarwal, S.; Lin, E. K.; Watkins, J. J. *Adv. Mater.* **2008**, *20*, 1603–1608.
(15) Koutsky, J. A.; Walton, A. G.; Baer, E. *J. Appl. Phys.* **1967**, *38*, 1832–1839.
(16) Nardini, M. J.; Price, F. P. *J. Phys. Chem. Solids* **1967**, *1*, 395–398.
(17) Price, F. P. *Fundam. Phenom. Mater. Sci.* **1966**, *3*, 85–103.
(18) Price, F. P.; Gornick, F. *J. Appl. Phys.* **1967**, *38*, 4182–4186.
(19) Reiter, G.; Sommer, J. U. *J. Chem. Phys.* **2000**, *112*, 4376–4383.
(20) Reiter, G.; Castelein, G.; Sommer, J. U. *Phys. Rev. Lett.* **2001**, *86*, 5918–5921.
(21) Reiter, G.; Castelein, G.; Sommer, J. U.; Röttele, A.; Thurn-Albrecht, T. *Phys. Rev. Lett.* **2001**, *87*, 226101.
(22) Reiter, G.; Sommer, J. U. *Phys. Rev. Lett.* **1998**, *80*, 3771–3774.
(23) Massa, M. V.; Dalnoki-Veress, K. *Phys. Rev. Lett.* **2004**, *92*, 255509.
(24) Massa, M. V.; Carvalho, J. L.; Dalnoki-Veress, K. *Phys. Rev. Lett.* **2006**, *97*, 247802.
(25) Carvalho, J. L.; Dalnoki-Veress, K. *Phys. Rev. Lett.* **2010**, *105*, 237801.
(26) Massa, M. V.; Dalnoki-Veress, K.; Forrest, J. *Eur. Phys. J. E: Soft Matter Biol. Phys.* **2003**, *11*, 191–198.
(27) Massa, M.; Carvalho, J.; Dalnoki-Veress, K. *Eur. Phys. J. E: Soft Matter Biol. Phys.* **2003**, *12*, 111–117.
(28) Loo, Y.-L.; Register, R. A.; Ryan, A. J. *Phys. Rev. Lett.* **2000**, *84*, 4120–4123.
(29) Loo, Y.-L.; Register, R. A.; Ryan, A. J.; Dee, G. T. *Macromolecules* **2001**, *34*, 8968–8977.
(30) Zhu, L.; Cheng, S. Z. D.; Calhoun, B. H.; Ge, Q.; Quirk, R. P.; Thomas, E. L.; Hsiao, B. S.; Yeh, F.; Lotz, B. *Polymer* **2001**, *42*, 5829–5839.
(31) Zhu, L.; Huang, P.; Chen, W. Y.; Ge, Q.; Quirk, R. P.; Cheng, S. Z. D.; Thomas, E. L.; Lotz, B.; Hsiao, B. S.; Yeh, F. *Macromolecules* **2002**, *35*, 3553–3562.
(32) Zhu, L.; Mimnaugh, B. R.; Ge, Q.; Quirk, R. P.; Cheng, S. Z. D.; Thomas, E. L.; Lotz, B.; Hsiao, B. S.; Yeh, F.; Liu, L. *Polymer* **2001**, *42*, 9121–9131.
(33) Huang, P.; Zhu, L.; Guo, Y.; Ge, Q.; Jing, A. J.; Chen, W. Y.; Quirk, R. P.; Cheng, S. Z. D.; Thomas, E. L.; Lotz, B.; Hsiao, B. S.; Avila-Orta, C. A.; Sics, I. *Macromolecules* **2004**, *37*, 3689–3698.
(34) Chen, H.-L.; Wu, J.-C.; Lin, T.-L.; Lin, J. S. *Macromolecules* **2001**, *34*, 6936–6944.
(35) Xu, J.-T.; Fairclough, J. P. A.; Mai, S.-M.; Ryan, A. J.; Chaibundit, C. *Macromolecules* **2002**, *35*, 6937–6945.
(36) Robitaille, C.; Prud'Homme, J. *Macromolecules* **1983**, *16*, 665–671.
(37) Sun, L.; Zhu, L.; Ge, Q.; Quirk, R. P.; Xue, C.; Cheng, S. Z. D.; Hsiao, B. S.; Avila-Orta, C. A.; Sics, I.; Cantino, M. E. *Polymer* **2004**, *45*, 2931–2939.
(38) Zhu, L.; Huang, P.; Chen, W. Y.; Weng, X.; Cheng, S. Z. D.; Ge, Q.; Quirk, R. P.; Senador, T.; Shaw, M. T.; Thomas, E. L.; Lotz, B.; Hsiao, B. S.; Yeh, F.; Liu, L. *Macromolecules* **2003**, *36*, 3180–3188.
(39) Hammond, M. R.; Mezzenga, R. *Soft Matter* **2008**, *4*, 952–961.
(40) Verploegen, E.; Zhang, T.; Jung, Y. S.; Ross, C.; Hammond, P. T. *Nano Lett.* **2008**, *8*, 3434–3440.
(41) Verploegen, E.; Zhang, T.; Murlo, N.; Hammond, P. T. *Soft Matter* **2008**, *4*, 1279–1287.
(42) Hamley, I. W.; Castelletto, V.; Lu, Z. B.; Imrie, C. T.; Itoh, T.; Al-Hussein, M. *Macromolecules* **2004**, *37*, 4798–4807.
(43) Hamley, I. W.; Castelletto, V.; Parras, P.; Lu, Z. B.; Imrie, C. T.; Itoh, T. *Soft Matter* **2005**, *1*, 355–363.
(44) Schneider, A.; Zanna, J.-J.; Yamada, M.; Finkelmann, H.; Thomann, R. *Macromolecules* **2000**, *33*, 649–651.
(45) Mao, G.; Ober, C. K. *Acta Polym.* **1997**, *48*, 405–422.
(46) Tenneti, K. K.; Chen, X.; Li, C. Y.; Shen, Z.; Wan, X.; Fan, X.; Zhou, Q.-F.; Rong, L.; Hsiao, B. S. *Macromolecules* **2009**, *42*, 3510–3517.
(47) Tenneti, K. K.; Chen, X.; Li, C. Y.; Wan, X.; Fan, X.; Zhou, Q.-F.; Rong, L.; Hsiao, B. S. *Soft Matter* **2008**, *4*, 458–461.
(48) He, X.; Sun, W.; Yan, D.; Liang, L. *Eur. Polym. J.* **2008**, *44*, 42–49.
(49) He, X.; Sun, W.; Yan, D.; Xie, M.; Zhang, Y. *J. Polym. Sci., Part A: Polym. Chem.* **2008**, *46*, 4442–4450.
(50) Bae, J.; Kim, J.-K.; Oh, N.-K.; Lee, M. *Macromolecules* **2005**, *38*, 4226–4230.
(51) Yu, H.; Piñol, T. *ACS Appl. Mater. Interfaces* **2009**, *1*, 2755–2762.
(52) Xu, B.; Piñol, R.; Nono-Djamen, M.; Pensec, S.; Keller, P.; Albouy, P.-A.; Lévy, D.; Li, M.-H. *Faraday Discuss* **2009**, *143*, 235–250.
(53) Yang, J.; Piñol, R.; Gubellini, F.; Lévy, D.; Albouy, P.-A.; Keller, P.; Li, M.-H. *Langmuir* **2006**, *22*, 7907–7911.
(54) Jia, L.; Cao, A.; Lévy, D.; Xu, B.; Albouy, P. A.; Xing, X.; Bowick, M. J.; Li, M.-H. *Soft Matter* **2009**, *5*, 3446–3451.
(55) Tao, Y.; Zohar, H.; Olsen, B. D.; Segalman, R. A. *Nano Lett.* **2007**, *7*, 2742–2746.
(56) Sackmann, E.; Meiboom, S.; Snyder, L.; Meixner, A.; Dietz, R. *J. Am. Chem. Soc.* **1968**, *90*, 3567–3569.
(57) Joo, S.-H.; Yun, Y.-K.; Jin, J.-I.; Kim, D.-C.; Zin, W.-C. *Macromolecules* **2000**, *33*, 6704–6712.
(58) He, Y.; Lodge, T. *Chem. Commun.* **2007**, 2732–2734.
(59) *Polymeric Nanostructures and Their Applications*, 2nd ed.; Nalwa, H. S., Ed.; American Scientific Publishers: Stevenson Ranch, CA, 2007; Vol. 1.
(60) Ahn, S.-K.; Deshmukh, P.; Kasi, R. M. *Macromolecules* **2010**, *43*, 7330–7340.
(61) Ahn, S.-K.; Deshmukh, M.; Osuji, C. O.; Kasi, R. M. *ACS Nano* **2011**, DOI: 10.1021/nn200211c.
(62) Soininen, A. J.; Kasëmi, E.; Schlüter, A. D.; Ikkala, O.; Ruokolainen, J.; Mezzenga, R. *J. Am. Chem. Soc.* **2010**, *132*, 113–177.
(63) Laiho, A.; Hiekkataipale, P.; Ruokolainen, J.; Ikkala, O. *Macromol. Chem. Phys.* **2009**, *210*, 1218–1223.
(64) Korhonen, J. T.; Verho, T.; Rannou, P.; Ikkala, O. *Macromolecules* **2010**, *43*, 1507–1514.
(65) Ikkala, O.; ten Brinke, G. *Science* **2002**, *295*, 2407.
(66) Li, C.; Schlüter, A. D.; Zhang, A.; Mezzenga, R. *Adv. Mater.* **2008**, *20*, 4530–4534.
(67) Epps, T. H.; Bates, F. S. *Macromolecules* **2006**, *39*, 2676–2682.
(68) Balsara, N. P.; Garetz, B. A.; Chang, M. Y.; Dai, H. J.; Newstein, M. C.; Goveas, J. L.; Krishnamoorti, R.; Rai, S. *Macromolecules* **1998**, *31*, 5309–5315.
(69) Yokoyama, H.; Kramer, E. J. *Macromolecules* **1998**, *31*, 7871–7876.
(70) Matsen, M. W.; Griffiths, G. H.; Wickham, R. A.; Vassiliev, O. N. *J. Chem. Phys.* **2006**, *124*, 024904.
(71) Matsen, M. W.; Bates, F. S. *Macromolecules* **1996**, *29*, 1091–1098.
(72) Chen, J.-Z.; Sun, Z.-Y.; Zhang, C.-X.; An, L.-J.; Tong, Z. *J. Chem. Phys.* **2008**, *128*, 074904.
(73) Liu, X.-B.; Zhao, Y.-F.; Chen, E.-Q.; Ye, C.; Shen, Z.-H.; Fan, X.-H.; Cheng, S. Z. D.; Zhou, Q.-F. *Macromolecules* **2008**, *41*, 5223–5229.
(74) Röttele, A.; Thurn-Albrecht, T.; Sommer, J.-U.; Reiter, G. *Macromolecules* **2003**, *36*, 1257–1260.
(75) Lai, J.; Filla, D.; Shea, R. *Macromolecules* **2002**, *35*, 6754–6756.
(76) Perrin, D. D.; Armarego, L. F. *Purification of Laboratory Chemicals*, 3rd ed.; Pergamon Press: Oxford, 1988.